Laser sintering of nano-hydroxyapatite coated polyamide 12 powders

D. Hui[a,b], R.D. Goodridge[a,b,*], C.A. Scotchford[a], D.M. Grant[a]

[a] *Advanced Materials Research Group, Faculty of Engineering, The University of Nottingham, University Park, Nottingham NG7 2RD, UK*
[b] *Additive Manufacturing and 3D Printing Research Group, Faculty of Engineering, The University of Nottingham, University Park, Nottingham NG7 2RD, UK*

ARTICLE INFO

ABSTRACT

As part of a larger study on the laser sintering (LS) of nano-composite structures for biomedical applications, a wet mixing method was used to coat Polyamide 12 (PA12) particles with nano-hydroxyapatite (nHA). The addition of nHA significantly affected powder processability due to laser absorption and heat transfer effects which led to part warping. This phenomenon has not been reported in other studies investigating LS of polymer/ HA and nHA powders. Nano-composites containing 0.5–1.5 wt% nHA were successfully produced and tensile testing showed that 0.5 wt% nHA provided the greatest reinforcement with a 20% and 15% increase in modulus and strength respectively. However, the elongation at break had significantly declined which was likely due to the formation of nHA aggregates at the sintering borders following the processing of the coated powders despite being initially well dispersed on the particle surface.

1. Introduction

The ability to construct highly complex, three dimensional (3D) structures from a variety of degradable and non-degradable polymers makes powder based additive manufacturing processes, such as laser sintering (LS), very promising in the field of bone tissue engineering. A laser (typically CO_2) acts on a preheated powder bed to selectively melt the surface of the polymer particles which fuses them together. Each consolidated layer corresponds to a 'sliced' image of a CAD model to be built [1]. When a layer is complete the build platform lowers and a new layer of polymer powder is spread over the previous layer and the process is repeated until the build is complete. LS has several key advantages over traditional methods for producing bone regenerative devices, such as sol–gel, gas foaming and particulate leaching. These include: control over internal and external geometries, part to part reproducibility, and no requirement for expensive moulds or potentially toxic binders associated with conventional methods [2–5].

Implants and devices that support migration, proliferation and differentiation of bone cells require a well interconnected, porous, 3D structure with modest mechanical strength, typically less than 2 MPa, in order to support the surrounding tissue whilst bone mineralisation occurs. Eventually the load will be transferred from the structure to the newly mineralised bone [6–13]. Structures made from composite materials such as polymer/inorganic fillers, are being increasingly explored for LS. The overall goal of this approach is to provide a combination of improved mechanical performance along with enhancing the bioactive properties of the fabricated structures. A popular choice of

filler is hydroxyapatite (HA: $Ca_{10}(PO_4)_6(OH)_2$) for bone tissue engineering applications due to its similar chemical composition to natural bone which promotes osteoblast adhesion, proliferation and differentiation. It is already being explored for use in polymer/composite powders for LS. For example, Hao et al. [14] and Zhang et al. [15] produced composite powders, of 20–40 vol% HA with polyethylene and polyamide to produce bone implant devices via LS. They did this by compounding the polymer and filler in a twin screw extruder followed by powderisation using a centrifugal mill. LS was then used to produce samples that exhibited rough, open porous structures with pore sizes ranging from 200 to 400 μm. The surface exposure of HA could be altered by increasing the laser power causing the vaporisation of material surrounding the HA particles. In vitro analysis using primary human osteoblasts (HOBs) showed that the addition of HA and LS processing provided surfaces with a favourable environment for cellular attachment, proliferation and ultimately led to improved bone mineralisation compared to neat polymers.

There has also been much focus on the utilisation of nano-particles (NPs) for bone tissue engineering devices. Due to their high specific surface area and nano-topography they can provide enhanced bioactivity when compared to micro-scale particles. In vitro cell studies by Webster et al. [16], who consolidated nanoparticles into disc shaped samples, demonstrated that osteoblast adhesion was significantly higher on nanoscale particles (24 nm alumina, 39 nm titania and 67 nm HA) compared to micron sized particles. Protein analysis also showed that NPs had greater levels of adsorbed vitronectin which is crucial for anchorage dependent cell attachment. Nano-hydroxyapatite (nHA) has

been successfully incorporated with polycarprolactone (PCL) powders by cryogenic freeze grinding and dry blending. LS was then used to produce nanocomposite scaffolds, for bone regeneration, which had 70–78% porosity and compressive strength improvements of 129% over neat PCL at 15 wt% loading of nHA [17]. Via SEM imaging, interconnected pores ranging from 600 to 800 μm could be observed which would allow for the exchange of fluids and penetration of osteoblasts and their precursors. Furthermore, in vitro cell studies, using human mesnchymal stem cells (hMSC), also showed that nHA/PCL scaffolds were more bioactive compared to neat PCL scaffolds with increased alkaline phosphatase (ALP) activity, bone mineralisation and an increased release of bone morphogenic protein 2 (rhBMP-2). In vivo studies using a rabbit model showed that the nHA/PCL (15 wt%) promoted increased levels of new bone formation compared to neat PCL scaffolds after 3, 6 and 9 weeks post surgery [17]. Other nHA/PCL scaffolds produced by LS have also been shown to possess increased surface hydrophilicity which was suggested to lead to improved cellular attachment [18]. Other systems used in LS include nHA/poly(L-lactic acid) (PLLA) and nano-carbonated hydroxyapatite (CHAp)/poly(hydroxybutyrate-co-hydroxyvalerate) (PHBV). Osteoblast like cells (SaOS-2) grown on these nanocomposite scaffolds had improved proliferation and ALP expression compared to cells grown on scaffolds made using neat polymer [19,20].

PA12 is the most commonly used polymer for LS. It is a semi-crystalline structure, with a narrow melting and crystallisation temperature range of 172–180 °C and 151–147 °C respectively. Due to its physical, thermal and chemical properties it is relatively easy to process via LS due to its wide processing window [21,5]. Furthermore, polyamide based materials have proven to be biocompatible with various human bone cell and tissue types and have been widely explored for use in non-degradable biomaterials [22–26]. For example, Qu et al. [27] showed that bone marrow stromal cells (BMSCs) grown on 4:6 wt% ratio of nHA/PA66 composite membrane, initially displayed higher cellular proliferation in comparison to the TCP control from 1 to 7 days. Zhang et al. [28] showed that 30 wt% HA/PA66 composite led to significantly higher proliferation of MG-63 cells after 7 days of culture in comparison to the tissue culture plastic (TCP) control. Hariharan et al. [29] demonstrated that a PA (grade not reported) substrate manufactured by LS and coated with HA by electron beam deposition lead to 22% and 45% higher cell growth by 7 and 15 days compared to untreated controls. Wang et al. [30] also showed that nHA/PA nanocomposite scaffolds made by phase inversion techniques displayed good bioactivity with in vitro and in vivo studies showing increased cellular proliferation and ALP expression and enhanced levels of new bone formation compared to neat PA scaffolds.

Conventional methods for powder production include solid-in-oil-in-water emulsion/solvent (S/O/W) techniques, the mixing of filler with polymer melts which are then extruded and cut into pellets before being cryogenically milled to form powders and dry blended with a filler. These methods of powder production have been utilised in the aforementioned examples. However, problems associated with these methods include: the agglomeration of the nano-fillers which can lead to poor mechanical properties compared to the neat polymer; the need for solvents; the angular shaped particles and wide size distributions associated with grinding/milling methods.

Therefore, the purpose of this study was to explore the use of an alternative powder production method to drastically increase the distribution and surface coverage of NP on individual polymer particles that when processed by LS will remain well distributed through out the structure and exposed on the surface. This method was previously used to coat individual PA12 particles with multi-walled carbon nanotubes (MWCNT) for laser sintering [31,32] but has been adapted for nHA. The morphology and thermal characteristics, in addition to processability of the coated powder, by LS, was examined.

2. Materials and methods

2.1. Preparation of coated polyamide powder

A commercially available LS polyamide 12 (PA12; PA2200) powder was obtained from EOS GmbH, Germany and an aqueous solution of rod shaped hydroxyapatite nanoparticles (nHA) from Promethean Particles Ltd, UK. The nHA had a typical length and diameter of 400 nm and 30 nm respectively. Individual PA12 particles were coated with nHA at six different loadings: 0.5, 1.0, 1.5, 2.0, 4.0 and 10.0 wt% using a method previously developed for coating PA12 powder particles with MWCNTs [33]. Briefly the method comprised of mechanically stirring a PA12/water colloid suspension to which another suspension of nHA/water, which had been sonicated for 15 min, was added. This was mixed at 80–90 °C for 30 min to allow the nHA to attach onto the surface of the PA12 particles. The coated powder was then filtered and dried in an oven overnight at 80 °C. Preliminary work with the nHA showed that loadings of 4.0 and 10.0 wt% powders could be prepared but could not be processed via LS. Neat PA12 (0 wt%) was used as a control and underwent the same production steps as the coated powders but with no nHA added. The 4.0 wt% nHA powders were analysed alongside: 0.5, 1.0, 1.5 and 2.0 wt% powders to demonstrate the effects of high nHA loadings on the physical, chemical and thermal characteristics of the powder. This may provide some information as to how the materials will behave during processing.

2.2. Particle sizing

Particle size analysis was conducted using a Mastersizer 3000 (Malvern) with an Aero S dry powder dispersion unit to feed the powder into the detector at a rate of 25% and an air pressure of 1 bar. A total of 10 measurements, were taken for each powder composition, at 5 s per reading. The results were then averaged. The powders were dried overnight in an oven at 80 °C prior to analysis.

2.3. Scanning electron microscopy

The morphologies of the coated PA12 powder particles and resulting laser sintered samples were examined under a scanning electron microscope (SEM). Samples were sputter coated with platinum for 180 s to produce a 30 nm coating and viewed in a Philips XL30 ESEM at 15–20 kV in hi vac mode.

2.4. Thermal characterisation

The thermal properties of the coated PA12 particles were analysed on a Perkin Elmer DSC800 ramping from 50 °C to 200 °C at 10 °C min^{-1}. Typical masses analysed were in the range of 7–10 mg. Thermogravimetric analysis, burn off test (TA Instruments Q500) conducted in air was also used to confirm the presence of the NPs at their respective weight percentages. A temperature scan programme from 50 to 800 °C in platinum pans and a ramp rate of 10 °C min was selected to burn off the polymer.

2.5. ATR-FTIR

The chemical characteristics of the neat PA12 powder and nHA coated PA12 powders were studied via attenuated total reflectance – Fourier transform infrared spectroscopy (ATR-FTIR) on a VERTEX 70/70v spectrophotometer (Bruker). As received neat PA12 and coated PA12 powders were analysed. Scanning was performed at a resolution of 8 cm^{-1} with a scan time of 1 min per sample over a range of 500–4000 cm^{-1}. Samples were scanned 3 times and the spectrum was acquired using the Bruker OPUS software.

2.6. X-ray diffraction

X-ray powder diffraction (XRD) studies on neat PA12, neat nHA and PA12 powders coated with nHA were conducted in a Siemens D500 diffractometer using Cu Kα radiation source (λ = 1.54 Å). The samples were recorded in 2θ from 15° to 100° with a step size of 0.5°. The resulting diffraction spectrum was then analysed using the Bruker EVA software.

2.7. Laser sintering of coated powders

The processing parameters for the 0–2 wt% coated PA12 powders were mapped using an EOS Formiga P100 laser sintering system. From preliminary work conducted (results of which are not reported here) it was found that the nHA-PA12 powders were most sensitive to build chamber temperature and energy density. The overall energy density input can be varied by changing laser power, scan speed or scan spacing [3,34]. For this particular nHA-PA12 powder, adjusting the energy density by either increasing laser power or decreasing scan speed had a similar effect. Therefore, in order to minimise the number of variables in this study, scan speed, scan spacing and layer thickness were kept constant at 2500 mm s^{-1}, 0.25 mm and 100 μm respectively. The build chamber temperature was varied from 160 °C to 177 °C (177 °C being the maximum temperature at which the powder could be spread across the build platform) and laser power was varied from 2 to 25 W which was the minimum and maximum power output for the machine. Small cuboidal (15 mm × 15 mm × 1 mm) test specimens were attempted. Tensile test specimensand 10 mm × 1 mm discs were fabricated using parameters which produced samples that had the least amount of curling and appeared to have good shape definition.

2.8. Mechanical testing

Tensile testing was conducted using an Instron uniaxial tensile tester with a 50 kN load cell and a video strain gauge. Tensile test specimens were sprayed with black paint to achieve a speckle pattern which allowed the video camera to track the sample. Five samples of each composition were tested at a rate of 1 mm s^{-1}. The elastic modulus, ultimate tensile strength (UTS) and elongation at break were then computed.

3. Results

3.1. Particle morphology and nanoparticle coverage

The uncoated PA12 powder had a near spherical morphology which can be seen in Fig. 1a. After coating with nHA this near spherical morphology was maintained with no noticeable alteration to the particle size and shape when compared to the original uncoated PA12 powder; this can be seen in Fig. 1b. The coating method also provided complete coverage around the particles with well dispersed nHA on the surface. Furthermore the level of particle coverage increased with increasing nHA loading and this can be seen in Fig. 2a–d which are magnified images of the uncoated, 1.0 wt%, 4 wt% and 10 wt% nHA-PA12 particles respectively. The SEM images of 0.5 wt 1.5 wt% and 2.0 wt% were excluded as it was difficult to distinguish any changes to the surface coverage. The 4.0 and 10.0 wt% powders clearly demonstrated that increased nHA loading offered significantly higher surface coverage.

The size distribution curve obtained from the mastersizer 3000 of the neat PA12 and a 4.0 wt% coated powder can be seen in Fig. 3. The neat PA12 powder had a D10, D50 and D90 of 34.9 μm, 53.7 μm and 82.3 μm respectively. Following the coating procedure, a relatively high loading of 4.0 wt% nHA had a similar size distribution with a D10, D50 and D90 of 35.4 μm, 54.7 μm and 84.0 μm respectively. As the 4.0 wt% powders did not significantly alter the overall particle size, the 0.5, 1.0, 1.5 and 2.0 wt% powders were excluded from the analysis.

3.2. Thermal analysis

Thermal analysis showed that the weight percentage remaining closely matched that of the applied concentration of nHA; this can be seen in Table 1. Small differences in loadings detected can be attributed to errors when measuring out the amount of nHA solution. The first heating and cooling cycles for all the powders displayed two distinct and separated melting and recrystallization peaks which were narrow as shown in Fig. 4. As the loading of the nHA was increased to 4 wt%, the crystallisation temperature increased by 8.6 °C compared to neat PA12.

3.3. ATR-FTIR analysis

ATR-FTIR was conducted on neat PA12 powder and PA12 powder coated with 0.5. 1.0, 2.0 and 4.0 wt% nHA and the results of these spectra can be seen in Fig. 5. Peak assignments can be seen in Table 3. The dotted lines show a distinct region where the CO_2 laser used on the LS system, with the wave-length of 10.6 μm, interacts with the polymer powder [35–37]. Within this region, the nHA coated powders show an additional peak located at 1032 cm^{-1} and this is reportedly associated with the PO_4^{-3} bending vibration. This is characteristic of hydroxyapatite and the intensity of this peak increases from 0.5 to 4.0 wt% nHA.

3.4. Laser sintering of coated PA12 powders

A process map of chamber temperature and laser power was produced and it can be seen in Fig. 6 that the increasing addition of nHA caused the processing window to significantly narrow compared to neat PA12 powder. The 0.5 wt% nHA-PA12 loading still maintained a relatively wide processing window; however at 1.0 wt% and 1.5 wt% this window narrowed significantly to the point where no combination of chamber temperature and laser power was suitable for producing completed builds at 2.0 wt% nHA. Based on visual observations, the
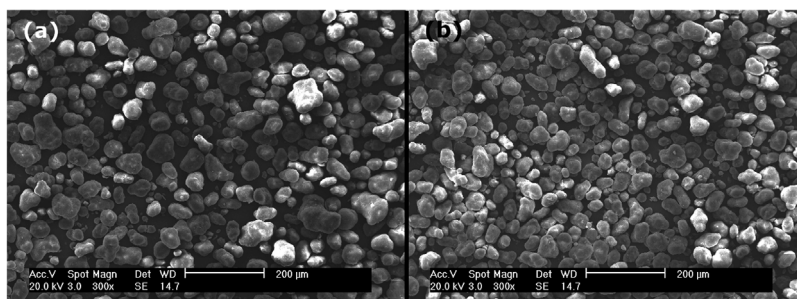

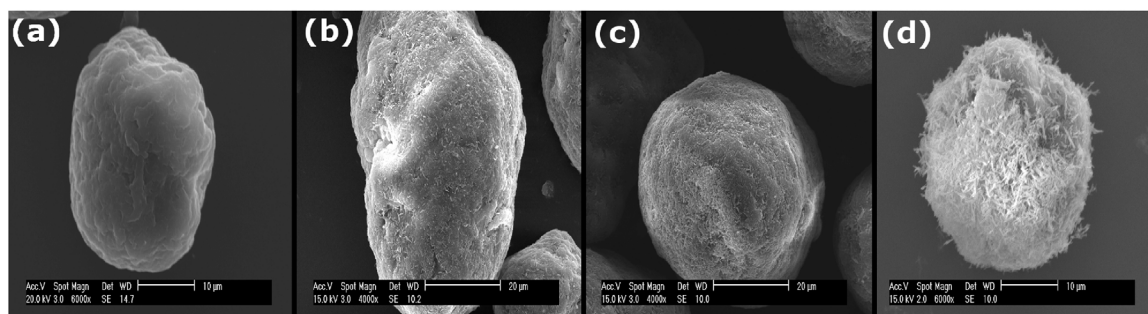**Fig. 1.** SEM images of (a) neat PA12 powder particles and (b) 4 wt% nHA-PA12.

Fig. 2. Magnified SEM images of (a) neat PA12 powder particle surface, (b) 1.0 wt% nHA-PA12, (c) 4 wt% nHA-PA12 particle surface, and (d) 10 wt% nHA-PA12 particle surface.
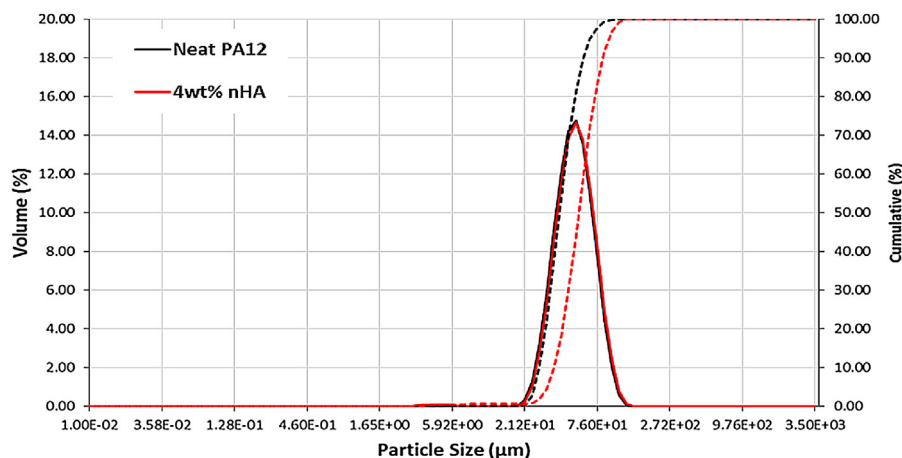

Fig. 3. Size distribution of neat PA12 and 4 wt% nHA coated PA12 particles. $N = 10$ per powder composition. Dotted lines represents cumulative volume (%).

Table 1
TGA data for neat and nHA-PA12 powders (mean values $n = 3$) using a ramp rate of $10\,°C\,min^{-1}$ in air. Error is reported as standard deviation.

Sample (wt% nHA)	Remaining (wt%)
Neat PA12	0.05 ± 0.02
0.5	0.46 ± 0.02
1.0	1.23 ± 0.04
1.5	1.41 ± 0.03
2.0	1.76 ± 0.03
4.0	3.90 ± 0.03

parameters that gave the least amount of curling and provided good shape definition for 0.5, 1.0 and 1.5 wt% nHA-PA12 powders, were a laser power of 20 W, 16 W and 10 W respectively and a build chamber temperature of 176 °C. These parameters were used to produce tensile test specimens and small disc shaped samples, as shown in Fig. 7a and b.

3.5. XRD analysis

Samples of neat PA12 powder, neat nHA, 1.0 wt% nHA coated powder and a 1.0 wt% sintered discs were recovered and analysed under XRD. The results of this test are displayed in Fig. 8. The neat PA12 powder is a semi crystalline polymer and therefore exhibits two strong crystalline peaks at $2\theta = 21.25°$ and $2\theta = 21.30°$ corresponding to d spacings of 0.412 nm and 0.400 nm respectively. The amorphous humps are also clearly visible appearing at 22° and 42°. The addition of 1.0 wt% nHA produces additional diffraction peaks at 25.86°, 31.78°, 32.18°, 32.91° and 34.06° for the coated PA12 powder, which correspond to the (002), (211), (112), (300) and (202) crystal planes. This is

characteristic of the hydroxyapatite mineral phase [38]. Intense peaks associated with these crystal planes are also visible on the pattern for neat nHA powder with additional characteristic HA peaks at $2\theta = 40.08°$, 46.98°, 49.78° and 53.50° corresponding to (130), (222), (213) and (004) planes respectively. The XRD pattern for the 1.0 wt% sintered discs shows a single intense peak located at $2\theta = 22.14°$ and a d spacing of 0.421 nm in addition to the faint presence of the (211), (112) and (300) HA crystal planes.

3.6. Mechanical testing

The tensile test data for each composition are shown in Table 4. The tensile properties for the 0.5 wt% nHA-PA12 sample compared to neat PA12 (20 W) were shown to be statistically significant with an increase in modulus and tensile strength of 20.0% and 15.0% respectively. The 1.0 wt% nHA-PA12 was also statistically significant with a modulus and tensile strength increase of 13.0% and 9.0% respectively compared to neat PA12 (20 W). However increasing nHA content to 1.5 wt% led to a 50.0% and 68.0% reduction in modulus and tensile strength compared to neat PA12 (20 W). The elongation at break for 0.5 and 1.0 wt% was also significantly lower than neat PA12 (20 W) samples, a difference of 46.0 and 44.0% respectively. However, no significant difference between 0.5 and 1.0 wt% samples was recorded. The 1.5 wt% nHA samples also showed a significant, 83.5%, drop in the elongation at break. When comparing the properties of neat PA12 processed at 20 W, 16 W and 10 W, despite the 16 W samples showing a slight decline in modulus, UTS and elongation at break these differences were not reported as being significant. The 10 W samples, on the other hand, did show a significant decline of 22.0%, 36.0% and 72.0% in modulus, UTS and elongation at break, respectively when compared to the 20 W samples. Fig. 9a shows that the fracture surface of the 0.5 wt% nHA-PA12, at low magnification, had a roughened surface with no apparent signs of
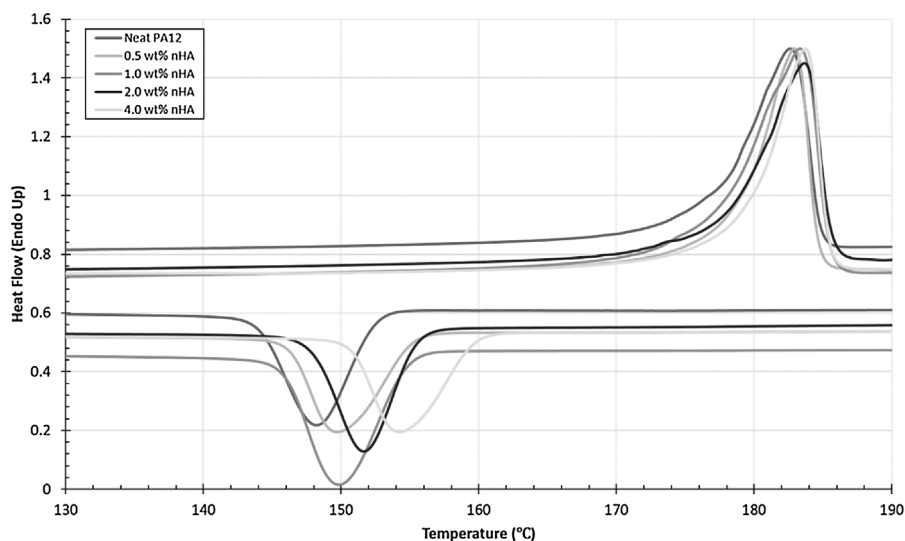
Fig. 4. Graph showing DSC curves of endothermic and exothermic phase changes during a heating and cooling cycle at 10 °C min^{-1} for neat PA12, 0.5 wt%, 1 wt%, 2 wt% and 4 wt% nHA loading.

Table 2
DSC data for neat and nHA-PA12 powders (mean values $n = 3$) using a ramp rate of 10 °C min^{-1}. Error is reported as standard deviation.

Sample	Tm (°C)	Tc (°C)
Neat PA12	183.7 ± 0.9	147.6 ± 2.8
0.5 wt% nHA	184.1 ± 1.0	149.9 ± 1.9
1.0 wt% nHA	183.5 ± 1.4	150.5 ± 0.2
2.0 wt% nHA	184.9 ± 0.6	153.7 ± 1.4
4.0 wt% nHA	183.7 ± 0.5	156.2 ± 0.3

Table 3
Assignment of FTIR spectrum for nHA coated PA12 powders.

FTIR peaks (cm^{-1})	Peaks assignment
3290 and 3094	N–H stretching and Fermi resonance
2917 and 2849	Asymmetric and symmetric stretching of CH_2
1638	C=O stretching is related to the amide I absorption band
1550	C–N stretching in addition to C=O in plane bending, collectively associated with the amide II band
1461 and 1368	CH_2 bending and CH bend and CH_2 twisting vibrations
1269	Amide III band due to C–N stretching and C=O in plane bending
1158	Skeletal motion involving CONH
1120	C–C stretching
946 and 716	CONH in plane bending and CH_2 rocking
620 and 538	N–H out of plane bending which is associated with the amide VI band
1032	PO_4^{-3} bending vibration of hydroxyapatite

plastic deformation; there are also visible signs of porosity within the structure. Increased magnification of the same surface as seen in Fig. 9b again reveals a roughed 'scale'-like surface texture orientated approximately 50° to the image plane and with no visible signs of extensive plastic deformation. The surface of the 1.0 wt% sample, in Fig. 9c, has a similar surface texture to the 0.5 wt% sample's fracture surface, however there are clear signs of partially sintered particles with micro-pits formed by their de-bonding. The higher magnification image in Fig. 9d shows the surface with more randomly orientated ridges with non uniform heights suggesting a slightly more ductile element of fracture occurred compared to the 0.5 wt% sample. Fig. 9e shows the fracture surface of the 1.5 wt% sample and shows clear signs of partially sintered particles leading to a large volume of voids present between the

layers. The higher magnification image in Fig. 9f shows signs of brittle fracture between the sintering necks on the partially sintered particles with large voids visible.
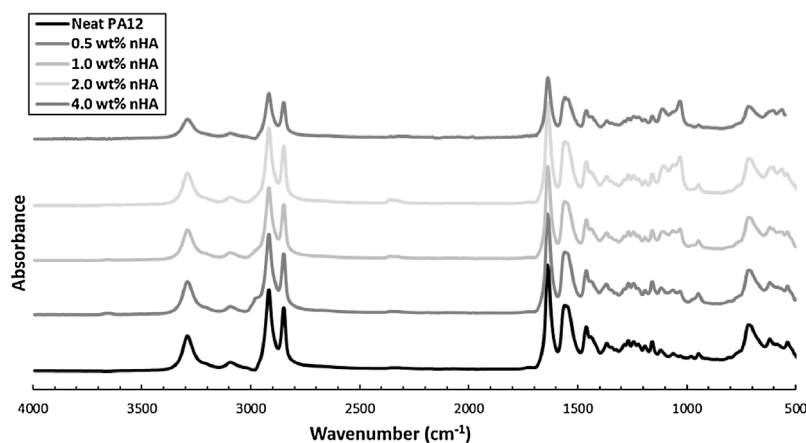

Fig. 5. ATR-FTIR spectrum of neat PA12, 0.5 wt% and 1 wt% nHA-PA12 powders. Dotted region depicts CO_2 laser interaction region.

Laser Power (W)

Fig. 6. A process map of neat PA12 and 0.5, 1.0, 1.5 and 2.0 wt% nHA-PA12 powders with varying laser power and build chamber temperatures. Solid grey box indicates completed builds with no curling. Diagonal lines indicate parameters which led to moderate curling and shifting of the build. Crossed lines show parameters which led to significant curling causing the build to fail on the first few layers.

Legend:
- Completed build
- Moderate curling or shifting of build leading to failure
- Significant curl causing build to instantly fail

Fig. 7. Images of (a) tensile test and (b) cell culture samples processed using different compositions of coated PA12 powders.

Fig. 8. XRD pattern for neat PA12, neat HA and 1.0 wt% coated PA12 powder and a 1.0 wt% nHA sintered disc. Neat HA has been indexed giving the (hkl) parameters.

Table 4
Table showing tensile test data for LS neat PA12 and nHA-PA12 nanocomposites, error is reported as standard deviation.

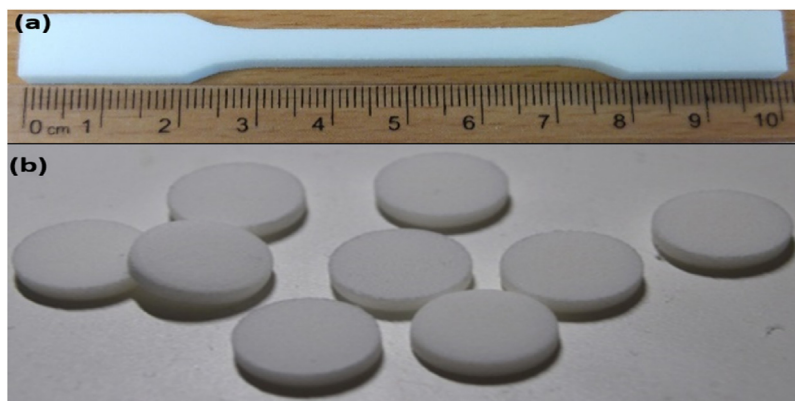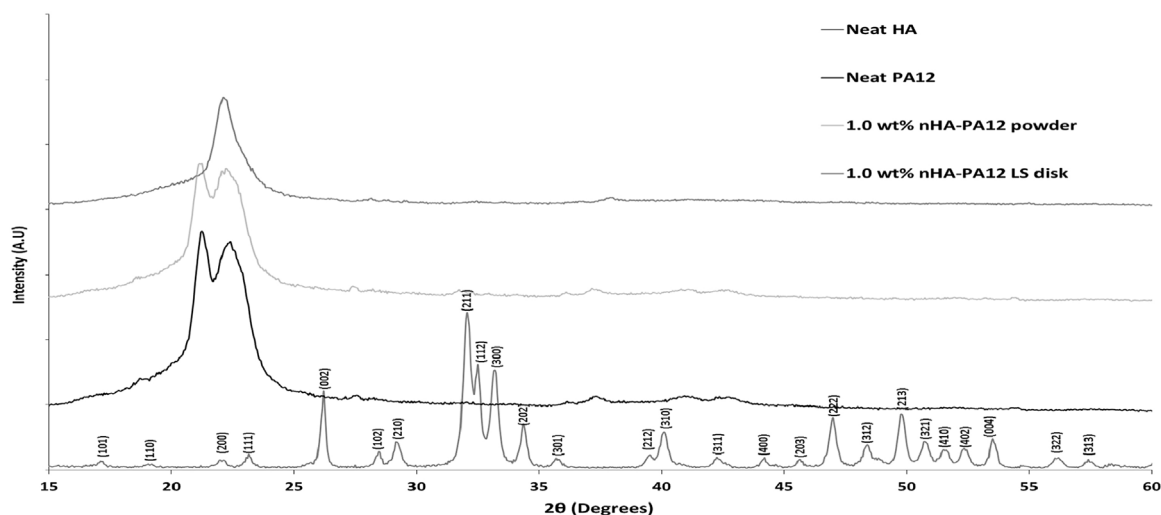| Sample	Young's modulus (GPa)	Ultimate tensile strength (MPa)	Elongation at break (%)
Neat PA12 (20 W)	1.43 ± 0.16	40.70 ± 0.23	23.60 ± 3.52
Neat PA12 (16 W)	1.32 ± 0.12	39.90 ± 0.33	20.51 ± 5.26
Neat PA12 (10 W)	1.11 ± 0.20	25.97 ± 6.77	6.64 ± 1.60
0.5 wt% nHA (20 W)	1.72 ± 0.02	46.76 ± 0.38	12.60 ± 1.84
1.0 wt% nHA (16 W)	1.63 ± 0.02	44.25 ± 0.54	13.20 ± 1.42
1.5 wt% nHA (10 W)	0.72 ± 0.09	12.90 ± 1.90	3.89 ± 3.94

4. Discussion

In laser sintering, the ability to deposit smooth uniform layers is crucial to the overall properties of the final part [39]. As mentioned previously, literature has shown that nHA has a high affinity for PA surfaces through the formation of –OH bonds between nHA and the active amide side groups of PA [40,41]. The procedure used to coat neat PA12 powder particles (Fig. 1) with nHA maintained the near spherical morphology of the original powder whilst providing a well dispersed and uniform coverage of nHA on the surface, as seen in Fig. 2. Achieving good dispersion of NPs is vital as large agglomerates can lead to a reduction of mechanical properties, such as fracture toughness, modulus and UTS, of the final part being produced [31]. Therefore the coating procedure adopted is well suited to the LS powders, as maintaining the spherical morphology has been shown to have improved flow performance and more efficient packing densities for PA12 and PA11 based powders in comparison to cryogenically milled/ground powders which have a more angular shaped morphology [39,5,42]. The particle size distribution is another important factor to consider with regards to the processability of the powders. Particle size can affect the flowability, surface finish, part accuracy and overall density of the part. Too small a particle size can lead to spreading difficulties due to static forces and may lead to part growth due to increased heat transfer [43,5]. Conversely too large a particle size can lead to poor surface finish and a shift of the processing window, requiring increased laser power to consolidate the particles due to the lower transfer of heat.

Therefore, particles should ideally have a relatively narrow size distribution between 45 and 90 μm [43]. The particle size distribution curve in Fig. 3 shows that the addition of nHA does not significantly affect the average size of the particle. Even with a relatively high loading of 4.0 wt% nHA, the coating method produced coated PA12 particles that maintained a narrow size distribution, with an average particle size of 54.70 μm, falling within the reported optimum range. This is indicative that the nHA was evenly dispersed over the particles and did not form large agglomerates on the surface. This was confirmed with the SEM images in Fig. 2.

In addition to powder morphology and size, the thermal properties of the powder are an important consideration as LS is a heat transfer process. Materials for LS ideally have a narrow melting range with no overlap of the melting and recrystallization peaks [21]. The DSC trace shown in Fig. 4a of neat and coated PA12 powders displays a prominent melting and crystallisation peak with a clear separation between the two. From Fig. 4a, the addition of nHA causes the average peak crystallization temperature to shift by 8.6 °C from 0 wt% loading to 4.0 wt% suggesting that the nHA has a strong heterophase nucleation effect. This phenomenon has been observed by Yan et al. [44] who coated PA12 powders with micron sized aluminium particles and observed an increase and narrowing of the crystallisation temperature range. Similar effects were also seen in nylon 6/clay nano-composites [45] and in PA12/MWCNT powders [33]. Therefore the addition of nHA has a significant effect on the thermal properties of the powder. This in turn has consequences on the processing parameters required to sinter the powder and to control thermal stresses during the build.

As seen in Fig. 6 the process maps for neat PA12 and 0.5–2.0 wt% nHA-PA12 show that the window for neat PA12 is very wide with completed builds from 165 °C at 2 W to 177 °C at 25 W. The addition of 0.5 wt% nHA causes the processing window to decrease slightly but still maintains a relatively wide processing window. However the process window becomes progressively narrower as the nHA content is increased to 1.0 wt% and 1.5 wt% with curling being more significant at lower build chamber temperatures. At 2.0 wt% nHA loadings completed builds were not successful due to in-build curling at all combinations of chamber temperature and laser power. Whilst other parameters could have been changed (e.g. scan speed, scan spacing and scan count) in an attempt to achieve completed builds, it was seen in preliminary work that alteration of these parameters did not improve the processability of the coated powder. Therefore this led to the general trend of a reduction in the processing window. It is clear from Fig. 6 that a relatively low addition of nHA has a significant influence on the ability to process the powder. A common trend observed is the increase in chamber
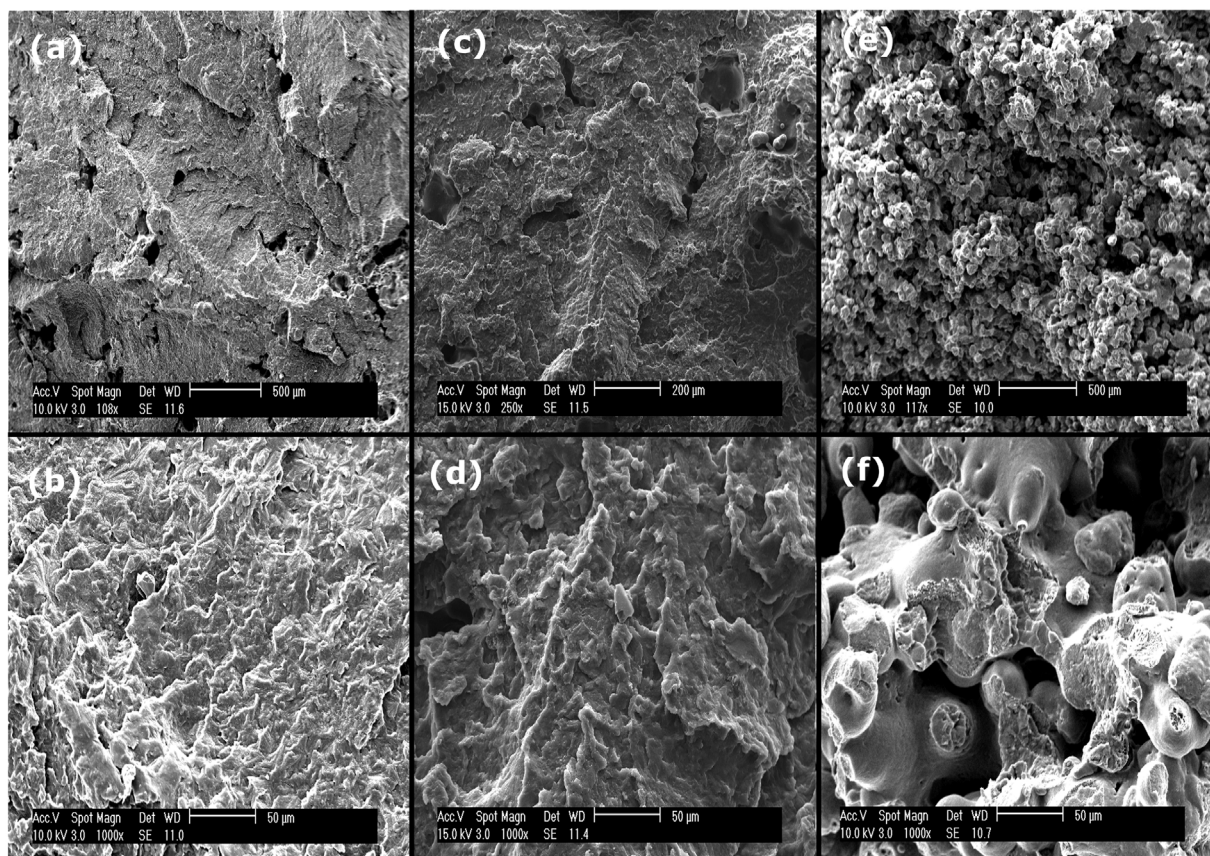
Fig. 9. SEM images of the fracture surfaces of 0.5 wt% (a) and (b), 1.0 wt% (c) and (d), and 1.5 wt% nHA-PA12 nanocomposites (e) and (f) taken at low and high magnifications respectively.

temperature required, with increasing nHA content, for successful builds. X-ray diffraction studies on the coated PA12 powders before and after sintering, as seen in Fig. 8, show the appearance of two distinct peaks at $2\theta = 21.25°$ and $21.30°$ for the un-sintered powder. These reflections have been reported to correspond to an unstable, monoclinic, α-phase [46,47]. Upon sintering this double peak collapses into a single intense peak at $2\theta = 22.14°$ and has been attributed to a more thermally stable γ-phase [46,47]. This transition from an unstable α-phase to a stable γ-phase (hexagonal) has been observed in other studies when observing the crystal structure of PA12 from melting to cooling [48,49]. This gamma phase reportedly provides toughness, to melt processed PA12, as it is believed to be more ductile and less stiff compared to the α-phase and thus influences much of the mechanical behaviour of the LS parts, which is discussed further below [50]. Furthermore, characteristic peaks associated with HA can also be seen, on both the coated PA12 powder and sintered discs, at $2\theta = 25.86°$, $31.78°$, $32.18°$, $32.91°$ and $34.06°$ corresponding to (002), (211), (112), (300) and (202) crystal planes [38]. These peaks are also present on the pattern for neat HA although the intensity is significantly higher compared to the coated powder due to the relatively low amount of nHA used to coat the PA12 particles. It is also evident on the pattern for the laser sintered disc that the localised temperature of the laser acting on the powder bed did not decompose HA to tri-calcium phosphate suggesting that localised heating well below 1000 °C and that the HA remained unaffected by the LS process [51].

The addition of HA has been known to influence the degree of consolidation in a variety of different composite systems. For example Hao et al. [14] found that HA had a significant effect on the degree of consolidation between HA/HDPE composite powders made by twin screw compounding and milling. Samples were processed using a CO_2 laser and at 58 wt% loadings a wide processing window was observed

for this material, however increasing the HA content to 63–78 wt% led to decreased levels of consolidation between polymer particles. In another study involving HA/PA composite powders made using the same technique by Savalani et al. [52] it was found that HA had a significant impact on the processability of the powders. The degree of fusion between polymer particles decreased with increasing HA loading and this was linked to the decline in specific heat capacity, of the composite powder when compared to the neat powder, which was speculated to lead to reduction of the heat penetration into the powder bulk. Work conducted by Zhou et al. [19] on LS of carbonated nHA/PLLA nanocomposite powders, made via S/O/W technique, also reported that HA acted as an "energy reservoir" based on specific heat capacity data. This decline in the degree of consolidation was also observed by XiaoHui et al. [53] who explored the processing of aliphatic HA/polycarbonate powders prepared by dry grinding and found that as the HA content increased from 5 to 15 wt% the porosity of the final part increased from 53 to 82% due to poor consolidation between particles.

CO_2 lasers are commonly employed in LS systems, the Formiga P100 used in this study has a CO_2 laser operating at 10.6 μm. HA strongly absorbs at this particular wavelength and this property of HA has been explored in the field of dentistry with the treatment of hypersensitive teeth caused by exposed dentin tubules using nHA pastes [54]. From Fig. 5 we can see that the dotted region represents the region in which the CO_2 laser interacts with the PA12 powder. With the addition of nHA a new peak, located at 1032 cm^{-1} emerges, the intensity of which increases with higher nHA content. This can be associated with the PO_4^{-3} bending vibration which is characteristic to HA.

However, from the examples mentioned above, the HA content that could be successfully processed was significantly higher than the loadings used in this study. The aforementioned studies utilised twin-screw compounding and milling and S/O/W emulsion/solvent

evaporation to produce composite powders therefore the HA was encapsulated within the polymer and perhaps did not have much interaction with the incoming laser. However this could not be the case with studies conducted by XiaoHui et al. [53] and Xia et al. [17] who both used dry blending techniques for powder production. This led to HA and nHA being deposited on the outside of the particles. However dry blending techniques generally lead to greater levels of NP agglomerates which could be observed in these studies and thus decrease the level of surface coverage provided. Again this leads to the conclusion that the nHA was much more evenly distributed on the surface of the PA12 particles in this study. Owing to the properties of NPs, such as high specific surface area compared to micron sized particles, the coating method used may have compounded the affect nHA has on the laser absorption and thermal characteristics of the powder due to the high degree of surface coverage and dispersion. This is further exacerbated by the fact that HA is strongly absorbing of CO_2 lasers in addition to being a poor thermal conductor. An example of this can be found in the work done by Wira et al. [18]; it was found that using fine HA particles in HA/PCL powder blends led to a higher degree of surface coverage of PCL particles and required increased energy input in order to sinter particles together compared to blends containing coarser HA particles. A combination of laser absorption by nHA and reduction in heat penetration through the sintered layers may potentially give rise to high thermal gradients and the development of curl. Curling becomes significantly worse and more difficult to control with the increasing addition of nHA. Often fine control over the build chamber temperatures and other parameters such as laser power can mitigate high thermal gradients and eliminate curl, however this approach failed when nHA content exceeded 1.5 wt%. This supports the theory that the high amount of energy absorption from the laser by the nHA layer means that localised heating on the nHA-PA12 particles results in the marked narrowing of the processing window as shown in Fig. 6.

The coating method used in this study was also used by Bai et al. [31,32] who coated individual PA12 polymers particles with MWCNT and by LS processing was able to successfully produce PA12/MWCNT nanocomposites. It was found that a relatively low amount of MWCNT could significantly improve the mechanical properties of the nanocomposite. In his study, a 0.1 wt% loading led to an increase in elastic modulus and tensile strength by 54.0% and 6.0% respectively, and without decreasing the elongation at break [31]. The author attributed the significant improvement in tensile properties to the high degree of dispersion of MWCNTs and increase in final part density of the sample; Bai observed a 4.1% increase in final part density. An increase in final part density is known to have a significant influence on the mechanical properties [55]. The combination of highly dispersed MWCNT and increased part density both contributed to significant reinforcement. In this work, the addition of nHA also led to an increase in both modulus and UTS. At 0.5 wt% loading a significant increase of 20.0% and 15.0% was observed for modulus and UTS, respectively. A 1.0 wt% load led to increases of 13.0% and 9.0%. However, a significantly higher degree of NPs was used in this work when compared to Bai's study, up to 15 times more. When comparing the modulus and UTS of neat PA12 samples

processed at 20 W and 16 W no significant differences were reported, however when processed at 10 W the tensile properties were significantly lower. This may suggest that the large increase in modulus and UTS observed for the 0.5 and 1.0 wt% nHA samples, which were also processed at 20 W and 16 W respectively, may be primarily due to the reinforcement of the relatively high quantity of nHA as opposed to any increase in final part density. SEM images of the fracture surfaces of both samples in Fig. 9(a and b) and Fig. 9(c and d) showed no obvious difference in terms of porosity. However, further measurements looking at the bulk density of the samples is needed to confirm this. The 1.5 wt % nHA samples, however, recorded a significant decrease in mechanical properties when compared to neat PA12. The affect that nHA had on the processing window for 1.5 wt% nHA-PA12 powders meant that a relatively low laser power (10 W) was required. The effects of which can be seen in Fig. 9e and f. The fracture surface of 1.5 wt% nHA-PA12 sample show a very low degree of consolidation between the particles compared to the 0.5 and 1.0 wt% nHA-PA12 samples. This low degree of particle consolidation contributed to a final structure which possessed a very low density, stiffness, strength and elongation at break.

It is also commonly reported that nanocomposites made by laser sintering see a notable decline in the elongation at break. For example, Salmoria et al. [56] who also produced PA/MWCNT nanocomposite by LS,at 0.5 wt% loading, observed a 9.0% and 31.5% improvement in modulus and UTS. However, the elongation at break decreased by 18.0%. Similar observations were made by Warnakula et al. [57], who produced PA12/nano Al_2O_3 nanocomposites, at loadings of 3, 5 and 10 wt%, via LS. The nanocomposites showed significantly improved UTS compared to neat PA12, however, the elongation dropped sharply by around 60–77%. Koo et al. [58] also observed significant reductions in the elongation at break for PA11/nanoclay and PA12/nanoclay in addition to PA11/carbon nanofibers and PA12/carbon nanofibers. This is in contrast to the study conducted by Bai et al. [31] who saw a significant increase in tensile and impact properties with no reduction in the elongation at break. Due to these positive results, the same powder production method as that used in Bai's study was adopted. However, the elongation at break, for both the 0.5 wt% and 1.0 wt% nHA samples, recorded a large decline of 47.0 and 44.0% respectively, which was more in line with the observations made above. The decline seen may be due to contact between the polymer particles. The packing state of the powder bed, prior to melting, will result in the adjacent surfaces of the polymer particles making direct contact with one another. Due to the NPs being relatively well dispersed on the surface of the polymer particles, the likelihood of NPs on the surfaces of adjacent polymer particles being in close proximity or even contacting each other is high. Once the powder was exposed to the laser, the particles coalesced forming necks between adjacent particles. The boundary between the polymer particles, or sintering border, may therefore have had a high concentration of agglomerated NPs. This is due to the high surface area to volume ratio and high surface energy associated with NPs, which makes them prone to forming aggregates. Once the powder was melted by the laser, the flow of material may have provided the opportunity for the NPs to reduce their surface energy by coalescing and forming
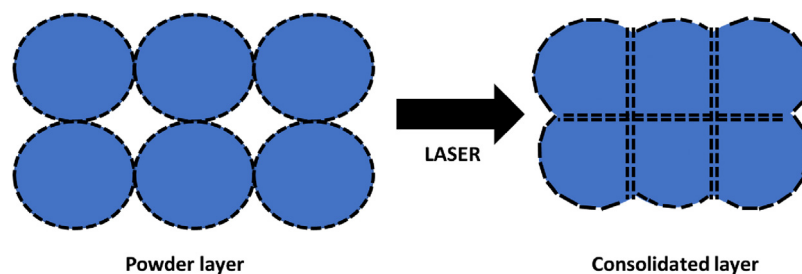

Fig. 10. Schematic showing consolidation of a powder layer. The dashed lines represent NPs. After laser energy is applied, the polymer particles coalesce and fuse together. At the sintering borders a high concentration of NPs can be seen; it likely that the NPs within these regions will be agglomerated.

agglomerates, especially at the sintering borders, this is depicted in Fig. 10.

This could have contributed to the reduction of the elongation at break by acting as defect sites when the final part was subjected to tensile loads [59]. TEM cross sectional analysis of PA12/MWCNT composites conducted in Bai's study [32] may support this notion. His study revealed a high density of MWCNT at the sintering borders between PA12/MWCNT particles. The loading of nHA used in this study was 10–15 times higher than that used in Bai's study. The high loading of nHA used may therefore have exacerbated the issue. In Bai's work the low quantity of 0.1 wt%, may have been below the loading threshold which would create sufficient agglomeration to negatively impact on the final part properties. He did note that when the MWCNT loading was increased to 0.2 and 0.4 wt% a higher degree of agglomerated particles could be seen. Achieving high dispersion within the bulk matrix is still a significant hurdle to overcome when trying to realise the full mechanical benefit that NPs can provide. However, this work does open further avenues for investigation of methods to maintain NP dispersion during LS in order to process higher NP loadings. This will be explored in future work.

5. Conclusion

The wet mixing method allowed for the production of nHA coated PA12 particles with a good distribution of nHA on the surface. The original, near spherical, morphology and narrow size distribution and was demonstrated using a 4 wt% nHA loading. However, the degree of dispersion and coverage caused difficulty in processing at low loadings, an affect that has not been reported in other studies utilising conventional powder production methods. Much higher loadings of HA have been successfully processed by LS. In this study, the high degree of particle coverage significantly reduced the processing window, with curling becoming increasingly significant with higher loadings of nHA, this could be due to a combination of laser absorption and heat transfer effects caused by the nHA on the surface of the polymer particles. This requires further detailed investigation to fully understand. Alternative nanoparticles which do not interact with CO_2 lasers are being investigated in the production of coated powder particles to further increase our understanding. The 0.5 and 1.0 wt% nHA loadings did, however, provide a reinforcing effect when compared to neat PA12 samples made using its optimised parameters. In this study there is a likely optimum loading of nHA for mechanical properties which lies between 0.5 and 1.0 wt% However, the elongation at break of nanocomposites decreased, in line with many observations made in literature on other nanocomposites prepared by LS. This is likely due to agglomeration of nHA occurring during powder melting. Exploring the use of coated nHA particles in an effort to maintain dispersion during processing will be explored in future work. The cellular response of osteogenic cells to PA12/nHA nanocomposite made using this method will also be explored in future studies.

References

[1] S. Shirazi, S. Gharehkhani, M. Mehrali, H. Yarmand, H. Metselaar, N. Kadri, N. Osman, A review on powder-based additive manufacturing for tissue engineering: selective laser sintering and inkjet 3D printing, Sci. Technol. Adv. Mater. 16 (3) (2015).

[2] S. Bose, S. Vahbzadeh, A. Bandyopadhyay, Bone tissue engineering using 3D printing, Mater. Today 16 (12) (2013) 496–504.

[3] A. Franco, M. Lanzetta, L. Romoli, Experimental analysis of selective laser sintering of polyamide powders: an energy perspective, J. Clean. Prod. 18 (16–17) (2010) 1722–1730.

[4] B. Caulfield, P. McHugh, S. Lohfeld, Dependence of mechanical properties of polyamide components on build parameters in the SLS process, J. Mater. Process. Technol. 182 (1–3) (2007) 477–488.

[5] R. Goodridge, C. Tuck, R. Hague, Laser sintering of polyamides and other polymers, Prog. Mater. Sci. 57 (2) (2012) 229–267.

[6] A. Salgado, O. Coutinho, R. Reis, Bone tissue engineering state of the art and future trends, Macromol. Biosci. 4 (8) (2004) 743–765.

[7] D. Hutmacher, Scaffold in tissue engineering bone cartilage, Biomaterials 21 (24) (2000) 2529–2543.

[8] P. Ma, Scaffolds for tissue fabrication, Mater. Today 7 (5) (2004) 30–40.

[9] T. Roy, J. Simon, J. Ricci, E. Rekow, V. Thompson, Performance of degradeabe composite bone repair products made via three-dimensional fabrication techniques, J. Biomed. Mater. Res. Part A 66A (2) (2003) 283–291.

[10] E. Harvey, J. Bobyn, M. Tanzer, G. Stackpool, J. Krygier, S. Hacking, Effect of flexability of femoral stem on bone-remodelling and fixation of the stem in canine total hip arthroplasty model without cement, J. Bone Joint Surg. 81 (1) (1999) 93–107.

[11] M. Kruyt, J. Bruijn, C. Wilson, F. Oner, C. Blitterswijk, A. Verbout, W. Dhert, Viable osteogenic cells are obligatory for tissue-engineered ectopic bone formation in goats, Tissue Eng. 9 (2) (2003) 327–336.

[12] Y. Kuboki, H. Takita, D. Kobyashi, E. Tsuruga, M. Inoue, M. Murata, N. Nagai, Y. Dohi, H. Ohgushi, Bmp-induced osteogenesis on the surface hydroxyapatite with geometrically feasible and nonfeasible structures: topology of osteogenesis, J. Biomed. Res. Part A 39 (2) (1998) 190–199.

[13] E. Tsuruga, H. Takita, H. Itoh, Y. Wakisaka, Y. Kuboki, Pore size of porous hydroxyapatie as the cell-substratum controls BMP-induced osteogenesis, J. Biochem. 121 (2) (1997) 317–324.

[14] L. Hao, M. Savalani, Y. Zhang, K. Tanner, R. Harris, Selective laser sintering of hydroxyapatite reinforced polyethylene composites for bioactive implants for tissue scaffold development, Proc. Inst. Mech. Eng. Part H 220 (4) (2006) 521–531.

[15] Y. Zhang, L. Hao, M. Savalani, R. Harris, L. Silvo, K. Tanner, In vitro biocompatibility of hydroxyaaptite-reinforced polymeric composites manufactured by selective laser sintering, J. Biomed. Res. A 91A (4) (2008) 1018–1027.

[16] T. Webster, C. Ergun, R.E.A. Doremus, Specific proteins mediate enhanced osteoblast adhesion on nanophase ceramics, J. Biomed. Mater. Res. 51 (3) (2000) 475–583.

[17] Y. Xia, P. Zhou, X. Cheng, Y. Xie, C. Liang, S. Xu, Selective laser sintering fabrication of nano-hydroxyapatie/poly-epsilon-carprolactone scaffolds for bone tissue engineering applications, Int. J. Nanomed. 8 (4) (2013) 4197–4213.

[18] F. Wiria, K. Leong, Y. Chua, C.K. amd Liu, Poly-epsilon-carprolactone/hydroxyapatite for tissue engineering scaffolds via selective laser sintering, Acta Biomater. 3 (2007) 1–12.

[19] W. Zhou, S. Lee, M. Wang, W. Cheung, W. Ip, Selective laser sintering of porous tissue engineering scaffolds from poly(ʟ-lactide)/carbonated hydroxyapatite nanocomposite microspheres, J. Mater. Sci. Mater. Med. 19 (7) (2008) 2535–2540.

[20] B. Duan, M. Wang, W. Zhou, W. Cheung, Z. Li, W. Lu, Three-dimensional nanocomposite scaffolds fabricated via selective laser sintering for bone tissue engineering, Acta Biomater. 6 (12) (2010) 4495–4505.

[21] J. Kruth, F. Levy, C.T.H.C. Klocke, Consolidation phenomena in laser and powder-bed based layered manufacturing, CIRP Ann. Manuf. Technol. 56 (2) (2008) 730–759.

[22] I. Springer, B. Fleiner, S. Jepsen, Y. Ail, Culture of cells gained from temporomandibular joint cartilage on non-absorbable scaffolds, Biomaterials 22 (2011) 2569–2577.

[23] H. Koji, T. Naohide, Y. Takafumi, T. Yoshinori, Prospects for bone fixation-development of new cerclage fixation techniques, Mater. Sci. Eng. C 17 (1–2) (2001) 19–26.

[24] D. Upadhyay, N.-Y. Cui, C. Anderson, N. Brown, A comparative study of the surface activation of polyamides using an air dielectric barrier discharge, Colloids Surf. A: Physicochem. Eng. Asp. 248 (1–3) (2004) 47–56.

[25] L. Hench, J. Wilson, Wiley Encyclopedia of Biomedical Engineering, John Wiley & Sons, Inc, 1993.

[26] W. Huanan, Y. Li, Y. Zuo, J. Li, S. Ma, L. Cheng, Biocompatibility and osteogenesis of biomimetic nano-hydroxyapatite/polyamide composite scaffolds for bone tissue engineering, Biomaterials 28 (22) (2007) 3338–3348.

[27] Y. Qu, P. Wang, Y. Man, Y. Li, Y. Zuo, J. Li, Preliminary biocompatible evaluation of nano-hydroxyapatite/polyamide 66 composite porous membrane, Int. J. Nanomed. 5 (2010) 429–435.

[28] X. Zhang, M. Lu, Y. Wang, X. Su, X. Zhang, The development of biomimetic spherical hydroxyapatite/polyamide 66 biocomposites as bone repair materials, Int. J. Polym. Sci. 2014 (2014) 6.

[29] K. Hariharan, G. Arumaikkannu, Influence of hydroxyapatite coated additive manufactured polyamide substrate on biocompatibility, Biomed. Res. 26 (4) (2015) 15–21.

[30] H. Wang, Y. Li, Y. Zuo, J. Li, S. Ma, L. Cheng, Biocompatibility and osteogenesis of biomimetic nano-hydroxyapatite/polyamide composite scaffolds for bone tissue engineering, Biomaterials 28 (22) (2007) 3338–3348.

[31] J. Bai, R.D. Goodridge, R.J.M. Hague, M. Song, Improving the mechanical properties of laser-sintered polyamide 12 through incorporation of carbon nanotubes, Polym. Eng. Sci. 53 (9) (2013) 1937–1946.

[32] J. Bai, R.D. Goodridge, R.J.M. Hague, M. Song, M. Okamoto, Influence of carbon nanotubes on the rheology and dynamic mechanical properties of polyamide-12 for laser sintering, Polym. Test. 36 (2014) 95–100.

[33] J. Bai, Development of a Polyamide 12/Carbon Nanotube Nanocomposite for Selective Laser Sintering (Ph.D. thesis), Wolfson School of Mechanical and Manufacturing Engineering, Loughborough University, 2013.

[34] A. Stwora, G. Skrabalak, Influence of selected parameters of selective laser sintering process on properties of sintered material, J. Achieve. Mater. Manuf. Eng. 61 (2) (2013).

[35] J. Han, Z. Cao, W. Gao, Remarkable sorption properties of polyamide 12 microspheres for a broad-spectrum antibacterial (triclosan) in water, J. Mater. Chem. A 1 (16) (2013) 4941–4944.

[36] S. Rhee, J. White, Crystal structure and morphology of biaxially oriented polyamide

12 films, J. Polym. Sci. B 40 (12) (2002) 1189–1200.

[37] I. Matsubara, Y. Itoh, S. Shinomiya, Lower-frequency infrared spectra (800–200 cm^{-1}) and structures of polyamides, J. Polym. Sci. B 4 (1) (1966) 47–53.

[38] R. Brundavanam, G. Poinern, D. Fawcett, Modelling the crystal structure of a 30 nm sized particle based hydroxyapatite powder synthesised under the influence of ultrasound irradiation from X-ray powder diffraction data, Am. J. Mater. Sci. 3 (4) (2013) 84–90.

[39] P.J. da Silva Bártolo, A.C.S. de Lemos, A.M.H, et al. (Eds.), Proc. 6th International Conference on Advanced Research in Virtual and Rapid Prototyping, CRC Press, Leiria, Portugal, 2013, p. 2013.

[40] X. Zhang, Y. Li, Y. Zuo, G. Lv, Y. Mu, H. Li, Morphology, hydrogen-bonding and crystallinity of nano-hydroxyapatite/polyamide 66 biocomposites, Compos. A: Appl. Sci. Manuf. 38 (3) (2007) 843–848.

[41] H. Kim, T. Furuya, T. Kokubo, T. Miyazaki, T. Nakamura, Composition of apatite produced in simulated body fluids, Key Eng. Mater. 218–220 (2001) 621–624.

[42] L. Verbelen, S. Dadbakhsh, M.V.E.A. Eynde, Characterization of polyamide powders for determination of laser sintering processability, Eur. Polym. J. 75 (2016) 163–174.

[43] R. Goodridge, K. Dalgarno, D. Wood, Indirect selective laser sintering of an apatite-mullite glass-ceramic for potential use in bone replacement applications, Proc. Inst. Mech. Eng. H: J. Eng. Med. 1 (220) (2006) 57–68.

[44] C. Yan, Y. Shi, J.E.A. Yang, Preparation and selective laser sintering of nylon-12-coated aluminum powders, J. Compos. Mater. (2009).

[45] L. Liu, Z. Qi, X. Zhu, studies on nylon 6/clay nanocomposites by melt intercalation process, J. Appl. Polym. Sci. 71 (7) (1999) 1133–1138.

[46] K. Inoue, S. Hoshino, Crystal structure of nylon 12, J. Polym. Sci. Polym. Phys. Ed. 11 (6) (1973) 1077–1089, http://dx.doi.org/10.1002/pol.1973.180110604.

[47] F. Xu, C. Yan, Y.-T. Shyng, H. Chang, Y. Xia, Y. Zhu, Ultra-toughened nylon 12 nanocomposites reinforced with IF-WS2, Nanotechnology 25 (32) (2014) 325701.

[48] M. Lon, J.C.G. Johnson, Solid-state nmr investigation of nylon 12, Macromolecules 24 (23) (1991) 6114–6122, http://dx.doi.org/10.1021/ma00023a011.

[49] C. Ramesh, Crystalline transitions in nylon 12, Macromolecules 32 (17) (1999) 5704–5706.

[50] S. Dasgupta, W. Goddard, W. Hammond, Crystal structures and properties of nylon polymers from theory, J. Am. Chem. Soc. 118 (49) (1996).

[51] C.-J. Liao, F.-H. Lin, K.-S. Chen, J.-S. Sun, Thermal decomposition and reconstitution of hydroxyapatite in air atmosphere, Biomaterials 20 (19) (1999) 1807–1813.

[52] M. Savalani, L. Hao, Y. Zhang, K. Tanner, R. Harris, Fabrication of porous bioactive structures using the selective laser sintering technique, J. Eng. Med. 221 (8) (2007) 873–886.

[53] S. XiaoHui, L. Wei, S. Pinghui, S. QingYong, W. QingSong, S. Yusheng, L. Kai, L. WenGuanh, Selective laser sintering of aliphatic-polycarbonate/hydroxyapatite composite scaffolds for medical applications, Int. J. Adv. Manuf. Technol. 81 (1) (2015) 15–25.

[54] M. Al-maliky, A. Mahmood, C. Al-karadaghi, M. Kurzmann, A. Laky, A. Franz, Moritz, The effects of CO_2 laser with or without nanohydroxyapatite paste in the occlusion of dentinal tubules, Sci. World J. (2014).

[55] N. Hopkinson, R. Hague, P. Dickens, Rapid Manufacturing: An Industrial Revolution for the Digital Age, John Wiley & Sons, 2006.

[56] G. Salmoria, R. Paggi, A. Lago, V. Beal, Microstructural and mechanical characterization of PA12/MWCNTS nanocomposite manufactured by selective laser sintering, Polym. Test. 39 (6) (2011) 611–615.

[57] A. Warnakula, S. Singamneni, Selective laser sintering of nano Al_2O_3 infused polyamide, Materials 10 (8) (2017) 864.

[58] J. Koo, S. Lao, W. Ho, K. Ngyuen, J. Cheng, L. Pilato, G. Wissler, M. Ervin, Polyamide nanocomposites for selective laser sintering, Proc. SFF Symp. Austin, 2006, pp. 392–409.

[59] P. Jain, P. Pandey, P. Rao, Selective laser sintering of clay-reinforced polyamide, Polym. Compos. 31 (4) (2010) 732–743.